Available online at www.sciencedirect.com
ScienceDirect
Journal of Geochemical Exploration 93 (2007) 160–176
JOURNAL OF GEOCHEMICAL EXPLORATION
www.elsevier.com/locate/jgeoexp

Mineralogy, geochemistry, and structural controls of a disseminated gold-bearing alteration halo around the schist-hosted Bullendale orogenic gold deposit, New Zealand

D.J. MacKenzie, D. Craw *, M. Begbie,

Geology Department, University of Otago, PO Box 56, Dunedin, New Zealand

Received 11 December 2006; accepted 9 April 2007
Available online 19 April 2007

Abstract

Orogenic gold-bearing quartz veins in the middle Tertiary Bullendale Fault Zone, New Zealand were mined historically for coarse gold in a narrow zone (ca. 5 m thick). However, recent drilling has revealed a broad hydrothermal alteration zone extending into the host schist, in which disseminated sulphide and gold mineralisation has occurred. The evidence of alteration is first seen over 150 m across strike from the fault zone, and the best-developed alteration halo is about 50 m wide. The extent and intensity of alteration is strongly controlled by local structures that developed during regional Tertiary kink folding of the pervasively foliated and fissile metasedimentary schist host. The earliest structures are foliation-parallel microshears (micron to millimeter scale) formed during flexural-slip folding. Later, but related, structures are predominantly normal faults and associated shear zones that have formed extensional sites during the regional folding event. All these structures facilitated hydrothermal fluid penetration and rock alteration, with localised vein formation and brecciation. Where fluid has followed structures, metamorphic chlorite, phengite, and titanite have been altered to hydrothermal ankerite, rutile, and muscovite or kaolinite. Ankerite with Fe/(Fe+Mg) <0.4 formed in host rocks with Fe/(Fe+Mg) of 0.6, and iron released by ankerite alteration possibly formed pyrite and arsenopyrite that host disseminated gold. Fault zones were extensively silicified and veined with quartz, albite, sulphides, and gold. Host rocks have wide compositional variations because of centimeter-scale metamorphic segregation. However, the alteration halo is characterised by elevated CO_2 and S, as measured by loss-on-ignition (doubled to ca. 6 wt.%), elevated As (100–10,000 ppm), and weakly elevated Sb (up to 14 ppm). Strontium is elevated and Ba depleted in many altered rocks, so Sr/Ba ratio increases from <1 (host rocks) to >3 in the most altered and silicified rocks. Many altered and mineralised rocks have low Sr/Ba (<0.5) as well. The subtle geochemical signature is not useful as a vector to ore because of the strong microstructural control on alteration. Likewise, there is no evidence for spatial mineralogical zonation across the alteration halo, although the most intense alteration is centred on the main fault zone, and intensity of alteration is controlled by microstructures at all scales. As documented in previous studies, hydrothermal alteration haloes enlarge the exploration target for some orogenic gold deposits, and may include disseminated gold, as in this Bullendale example.

Keywords: Hydrothermal; Mesothermal; Ankerite; Sulphide; Geochemistry; Fault; Shear; Fold

1. Introduction

Turbidite-hosted mesothermal (orogenic) vein-hosted gold deposits have traditionally been assumed to have negligible wall rock alteration zones, but

* Corresponding author.
E-mail address: dave.craw@stonebow.otago.ac.nz (D. Craw).

0375-6742/$ - see front matter © 2007 Elsevier B.V. All rights reserved.
doi:10.1016/j.gexplo.2007.04.001

research in the past 20 years has shown that these deposits typically have hydrothermal alteration haloes (e.g., Böhlke, 1988; Eilu and Mikucki, 1998; Bierlein and Crowe, 2000; Bierlein et al., 2000). Recognition of the existence of alteration zones is important, as this increases the size of the target mineralised zone during mineral exploration (Bierlein and Crowe, 2000). Also, some of the altered host rocks contain anomalous (ppm scale) concentrations of gold, far-removed (metres to tens of metres) from the main vein zones (Böhlke, 1988; Eilu and Mikucki, 1998; Craw et al., 1999). Thus, the volume of potential ore may be greater when alteration zones can be identified (Craw et al., 1999). This has led to the development of the concept of large tonnage, low-grade mesothermal gold deposits that include mineralised host rock as well as the narrow mineralised quartz veins that have traditionally been the focus of mining (Bierlein and Maher, 2001; Christie and Brathwaite, 2003; Goldfarb et al., 2005; Mitchell et al., 2006).

Mesothermal gold deposits typically form during compressional or transpressional tectonics (Kontak et al., 1990; Cox et al., 1991; Bierlein and Crowe, 2000; Goldfarb et al., 2005). Mineralisation in these deposits commonly occurs while the host rocks were being folded and/or reverse-faulted (Sibson et al., 1988; Cox et al., 1991; Goldfarb et al., 2005). Veins form in local extensional sites centred on well-defined fractures in host rocks (Sibson et al., 1988; Cox et al., 1991). Most host rocks are competent and massive on the metre to ten metre scale during mineralisation, so fluid flow was controlled by well-defined fractures in these competent rocks, with minor leakage of fluid into host rocks along, for example, grain boundaries and micro-fractures (Cox et al., 1991; Witt and Vanderhor, 1998). The competent, relatively impermeable host rocks generally resist development of alteration zones, and ensure that the alteration zones are subtle (Gray et al., 1991; Phillips and Powell, 1993). The structures that controlled fluid flow were sporadically developed and were commonly obscured by alteration reactions. Hence, detailed structural control on hydrothermal alteration of host rocks in mesothermal gold deposits has been little-described previously.

This study reports on the nature of the structural control, and the resulting mineralogical and geochemical alteration, of hydrothermal fluid penetration into host rocks adjacent to the Bullendale mesothermal gold deposit in southern New Zealand (Craw et al., 2006). Unlike most mesothermal gold deposits, the deposit we describe is geologically young (middle Tertiary), and was formed relatively close (<5 km) to the palaeosurface. This deposit has had negligible structural overprinting, and the details of hydrothermal fluid flow and alteration are still preserved. Further, the deposit is unusual in that it is hosted in highly fissile rocks that are layered on the millimetre to centimetre scale. This extreme fissility has resulted in locally near-pervasive formation of structurally-controlled fluid pathways through the rock. These provide graphic examples of development of enhanced fluid flow zones during compressional deformation, at a much smaller scale than is normally observed in mesothermal deposits. Despite the well-developed alteration zones associated with this mesothermal gold deposit, there has been little change in bulk rock composition, and hydrothermal alteration reactions were primarily controlled by mineralogical changes. We document the structural and mineralogical changes during mineralisation as an example of an enlarged exploration target and potential ore zone, features that are relevant to all exploration programmes targeting mesothermal gold-bearing vein and/or disseminated systems.

2. General geology

2.1. Structure of host rocks

The mesothermal system that is the focus of this study, the Bullendale deposit, is hosted in Mesozoic Otago Schist metasedimentary rocks of southern New Zealand (Mortimer, 1993) (Fig. 1). The host rock is pervasively deformed and recrystallised metagreywacke and meta-argillite, with no sedimentary features preserved. The rocks were subjected to at least two phases of isoclinal folding during greenschist facies metamorphism (Craw, 1985). Associated development of pervasive foliations was accompanied by progressive recrystallisation of coarse grained (>100 μm) muscovite and chlorite (Turnbull et al., 2001). This penetrative fabric is a composite feature, defined by convergence of at least two synmetamorphic foliations (Craw, 1985). Foliation development was accompanied by metamorphic segregation and formation of synmetamorphic quartz-albite veins that have been rotated into parallelism with the micaceous fabric, resulting in highly fissile rock with alternating (milllimetre to centimetre scale) micaceous and quartzofeldspathic layers (Fig. 2A and B). Metamorphic calcite, epidote and titanite occur throughout the rocks, particularly in the micaceous layers (Fig. 2A and B). Minor (1–10 m scale) metabasites are intercalated with the metasedimentary rocks, and have similar fabric development, with less quartz. The pervasive metamorphic fabric in the schist was formed subhorizontally during Jurassic orogenesis, and this

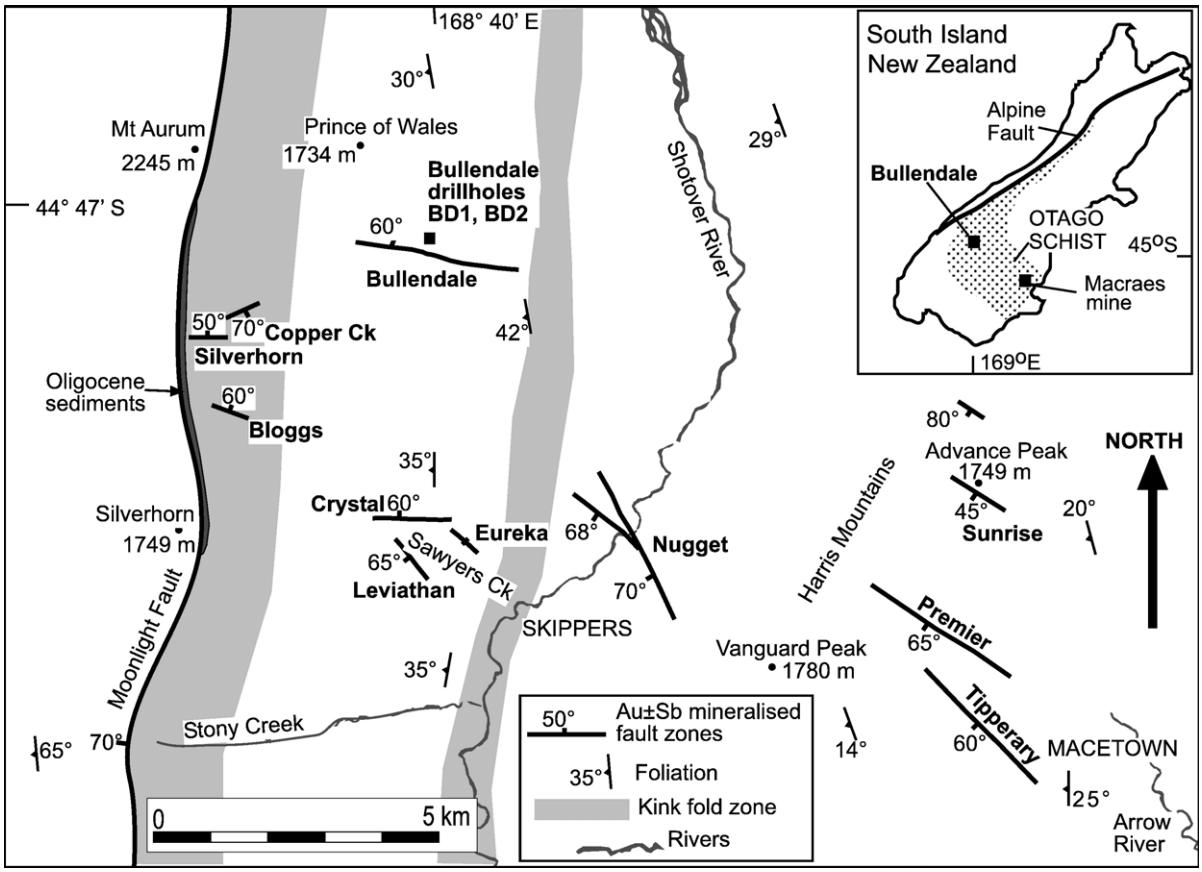

Fig. 1. Geological map of the area surrounding the mineralised Bullendale Fault Zone, showing the regional structure, associated mineralised zones, and location of the drillholes described in this study. Inset shows the location of the area in the Otago Schist in the South Island of New Zealand.

fabric is still subhorizontal over most of the ca. 40,000 km^2 of the Otago Schist (Mortimer, 1993). The subhorizontal fabric was uplifted with negligible rotation during Jurassic–Cretaceous exhumation (Mortimer, 1993; Gray and Foster, 2004). Mesothermal gold mineralisation accompanied the Jurassic–Cretaceous exhumation, including the large (>6 Moz) Macraes deposit (Fig. 1; Craw, 2002; Mitchell et al., 2006).

The western portion of the Otago Schist belt was redeformed in the Miocene during initiation of the current convergent plate boundary that now occurs on land as the Alpine Fault (Fig. 1; Cooper et al., 1987). Compressive deformation resulted in regional-scale disruption of the flat-lying foliation by north to northeast trending upright folds and reverse faults (Fig. 1; Craw, 1985; Cooper et al., 1987). The most prominent of these structures is the Moonlight Fault (Fig. 1), a regional-scale west-dipping reverse fault. This fault developed by reactivation of a pre-existing structure, along which Oligocene marine and non-marine sediments had been deposited (Turnbull et al., 1975). Remnants of these sediments are preserved along the Moonlight Fault (Fig. 1), and they were folded and faulted during the Miocene deformation. Folds of sediments continue into the structurally underlying fissile schist, as zones of open to tight upright kink folds of foliation (Fig. 2A and B), on all scales from centimetres to tens of metres. The kink-folded zones are up to 2 km wide (Fig. 1) with variable fold intensity.

2.2. Middle Tertiary gold mineralisation

A swarm of mineralised zones formed during the development of the Moonlight Fault and associated fold zones in the middle Tertiary (Cooper et al., 1987; Craw, 1989; Craw et al., 2006). This swarm trends SE from the Moonlight Fault to Macetown (Fig. 1). The mineralised zones contain auriferous pyrite, arsenopyrite, and quartz. Some mineralised zones contain stibnite, but there is little or no gold directly accompanying stibnite. Many of these mineralised zones have been mined historically, with the Bullendale Fault Zone being the most prominent

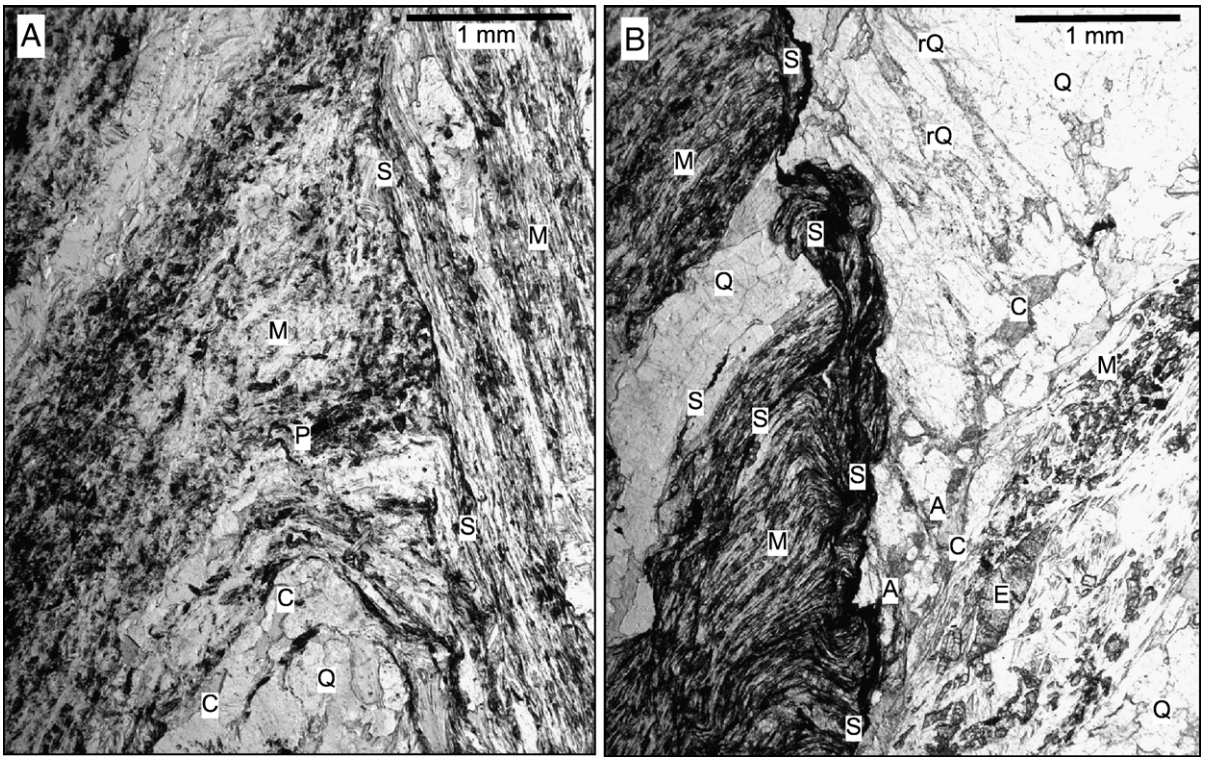

Fig. 2. Photomicrographs of folded and incipiently altered host schist. The schist was strongly segregated during metamorphism into quartz-rich (white, Q) and muscovite-rich (grey, M) laminae. Chlorite (C) and epidote (E) occur in both types of laminae. Metamorphic pyrite (P) occurs locally in micaceous laminae. Flexural slip deformation during folding has resulted in foliation-parallel microshears (black, S) that locally truncate foliation in fold hinges. Image A (BD2, 81.5 m) shows only incipient development of microshears in a micaceous layer. Image B (BD1, 93.5 m) has more prominent shears in micaceous layers, some associated shears with hydrothermally recrystallised quartz (grey, rQ), and minor replacement of chlorite by ankerite (A).

(Williams, 1974; Begbie and Craw, 2006). The Bullendale mine produced >30,000 oz of gold with grades of ca. 0.5 oz/tonne, from a narrow (typically <5 m thick) quartz lode system before closing in the early 1900s (Williams, 1974; Begbie and Craw, 2006).

Most of the gold and stibnite mineralisation was initiated during the early stages of kink fold development, and some mineralised zones are folded (Craw et al., 2006). Historic mines, including Bullendale, were developed in mineralised normal faults at a high angle to, and crosscutting, the Moonlight Fault related folds (Fig. 1). These extensional structures that host some mineralised zones formed in response to the regional middle Tertiary compression during initiation of the Alpine Fault (Cooper et al., 1987; Craw et al., 2006). Miocene lamprophyre dykes fill similarly-oriented structures a few kilometres to the north of the mineralised swarm (Craw, 1985; Cooper et al., 1987; Craw et al., 2006). Associated near-surface diatremes were emplaced at the same time (Cooper, 1986; Craw, 1985). Fluid inclusions in gold-bearing veins near Sawyers Creek (Fig. 1) also confirm the shallow-moderate emplacement level of these structures, with fluid immiscibility implying mineralisation at 2–4 km depth and 150–200°C (Craw, 1989; Craw and Norris, 1991).

The locus of orogenic deformation and uplift evolved northwards in the Miocene to present, and the mineralised zones exposed near the Moonlight Fault have not been overprinted by later structural events (Craw et al., 2006). The Moonlight Fault is still active, but Quaternary movement has been on the scale of metres only (Turnbull, 2000). The mineralised area is rugged, with high relief (>1000 m), steep slopes, and deeply-incised gorges.

3. Methods

This study focuses on the Bullendale Fault Zone (Fig. 1), where two cored drillholes provide almost-continuous clean and unoxidised exposure through unaltered and hydrothermally altered rock adjacent to the mineralised zone. The unoxidised rock exposed in

these cores is a key feature of the material, as surface exposures are invariably weathered to some extent, despite the high relief and actively-eroding slopes. The two cored holes (BD1, BD2; Fig. 3) were drilled in 1997 as part of an exploration programme reinvestigating the Bullendale Zone (Begbie and Craw, 2006). Seventy samples (ca. 250 g each) deemed to be representative of altered and unaltered rock were taken from key points in the cores. Both cored holes finished in altered rock (Fig. 3), so most sampling was focused on the transition with depth from unaltered to altered rock as the mineralised zone was approached, then to silicified rocks in fault zones. X-ray fluorescence analyses (major and selected trace elements) of subsamples (ca. 100 g) were obtained from SpectraChem Ltd (Wellington, New Zealand), accredited by International Accrediation New Zealand. Detection limits for trace elements are ca. 1 ppm. Small aliquots (ca. 20 g) of remnant powders from these subsamples were analysed for Ag, Sb, and Bi by ALS-Chemex (Brisbane, Australia), which has ISO 9001: 2000 registration and NATA accreditation. These latter metals were analysed by ICP-MS after acid digestion, with detection limits of 0.02 (Ag), 0.01(Bi) and 0.05(Sb) ppm. Additional analyses for As (atomic absorption) and Au (fire assay, AA finish) through the most mineralised zone were obtained from an unpublished company report. Detailed logging of the core in hand specimen yielded a mineralogical paragenetic sequence of alteration, and this was supplemented with transmitted and incident light petrography. Mineral compositions were determined with a JEOL JXA-8600 microprobe in the Geology Department,

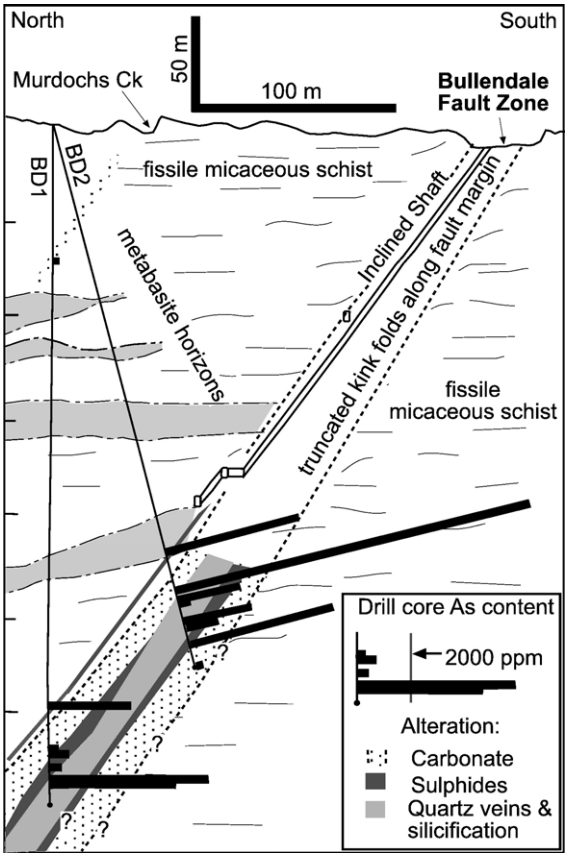

Fig. 3. Cross section through the Bullendale Fault Zone (after Begbie and Craw, 2006) showing the historic underground workings and the locations of the drillholes BD1 and BD2. Rocks with abundant hydrothermal minerals (as indicated) are shown in the main alteration zone, and histograms of As concentrations are based on the drillhole lines.

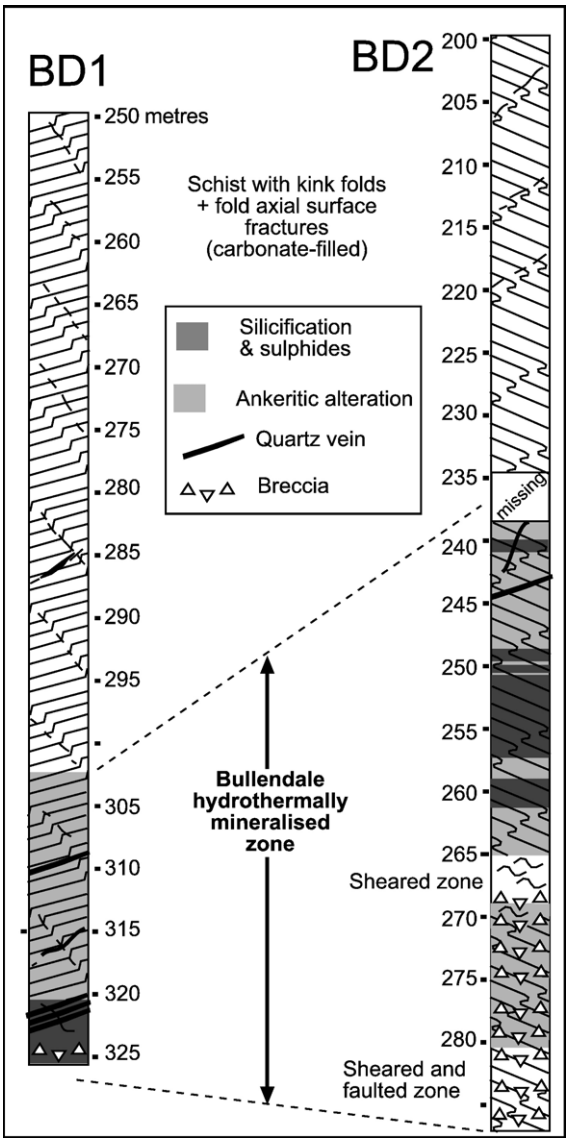

Fig. 4. Core logs through the most mineralised portions of the drillholes, showing the principal alteration rock types that occur in the Bullendale alteration halo, and the scales of their distribution.

University of Otago. The operating conditions for silicates were 15 kV accelerating voltage and 20 nA specimen current, with beam size between 20 and 10 μm. Oxide and silicate mineral standards were used for calibration. Arsenopyrite was analysed at 25 kV and 20 nA specimen current, using 100 s counting time, with Santa Eulalia arsenopyrite as a standard.

4. Bullendale Fault Zone and alteration halo

The Bullendale cores, BD1 and BD2, are 326 m and 287 m long respectively (Figs. 3 and 4). Most of the cores are barren fissile metasedimentary schist with subordinate metabasite horizons (Fig. 3). The pervasive foliation dips moderately west (Fig. 1) and is sporadically disrupted by folds (Fig. 2). Metabasite horizons are readily correlated along strike in the N–S plane of intersection of the drillholes (Fig. 3). Apart from a narrow zone of alteration at 50–70 m depth, altered rocks are not encountered until ca. 300 m in hole BD1 and nearly 240 m in hole BD2 (Figs. 3 and 4). The hydrothermally altered and mineralised zone below these depths is up to 50 m thick measured perpendicular to the Bullendale Fault Zone (Fig. 3). Alteration shows up as ankerite-rich zones, sulphide-bearing zones, and variably developed veins, breccias and silicification zones (Figs. 3 and 4). Mineralised rocks are variably enriched in arsenic (Fig. 3; Table 1), forming a halo around the Bullendale Fault Zone (Figs. 3 and 4). The halo is also discernible in hand specimen as light brown ankerite is visible locally.

Table 1
Representative geochemical analyses of unaltered (U), altered (A), and silicified (S) schists from drillholes (Fig. 3) through the Bullendale alteration halo

Hole	BD1	BD1	BD1	BD1	BD1	BD1	BD1	BD2	BD2	BD2	BD2
Depth, m	52.4	115.8	196.5	286.4	323	325	317.3	243.8	244.5	255	257
Alteration	U	U	U	A	A	A	A	S	S	S	S
SiO_2	64.07	58.97	70.77	65.97	67.91	57.93	66.00	90.81	78.05	88.63	93.44
Al_2O_3	15.38	17.32	13.72	12.93	12.87	19.95	14.02	2.48	3.71	4.36	2.48
Fe_2O_3	5.25	5.81	3.53	3.67	3.90	4.83	3.62	1.38	3.32	1.18	0.62
MnO	0.08	0.09	0.05	0.08	0.06	0.05	0.06	0.02	0.13	0.02	0.01
MgO	1.95	2.16	1.21	0.73	1.43	1.43	1.31	0.58	1.37	0.60	0.40
CaO	4.14	4.73	2.28	5.08	2.27	1.61	2.55	1.15	4.77	0.91	0.67
Na_2O	3.56	3.30	3.63	5.23	1.74	2.24	4.18	0.66	0.81	1.69	1.10
K_2O	1.88	2.88	2.46	1.09	2.53	3.33	2.61	0.35	0.65	0.32	0.08
TiO_2	0.67	0.75	0.41	0.49	0.50	0.92	0.51	0.09	0.13	0.11	0.05
P_2O_5	0.15	0.19	0.13	0.30	0.08	0.16	0.11	0.02	0.31	0.01	0.01
LOI	2.68	3.49	1.64	3.83	5.01	6.17	4.59	1.88	6.27	1.68	1.21
Total	99.80	99.69	99.83	99.42	98.31	98.61	99.56	99.42	99.52	99.51	100.06
As	14	7	3	3172	6190	4907	398	2434	356	2628	1211
Ba	581	906	610	253	480	680	632	90	153	77	57
Ce	35	56	38	63	68	128	52	7	20	5	2.5
Cr	31	43	8	19	27	73	21	<0.5	<0.5	<0.5	<0.5
Cu	25	30	14	10	29	22	9	1	<0.5	4	<0.5
Ga	17	20	14	17	18	28	18	<0.5	<0.5	<0.5	<0.5
La	17	31	8	21	29	65	30	<0.5	<0.5	<0.5	<0.5
Nb	8	11	8	10	9	17	10	4	5	4	3
Ni	14	14	5	9	7	21	5	<0.5	1	<0.5	<0.5
Pb	26	24	15	41	21	20	33	15	34	22	7
Rb	64	109	91	39	103	136	103	13	23	11	2
Sr	441	564	303	845	518	847	259	179	648	176	133
Th	0.5	13	<0.5	22	31	35	15	<0.5	<0.5	<0.5	<0.5
U	0.5	<0.5	<0.5	<0.5	<0.5	<0.5	<1	<0.5	<0.5	<0.5	<0.5
V	108	126	62	78	87	149	94	23	25	36	<0.5
Y	20	21	12	19	20	31	20	2	9	3	1
Zn	67	82	53	77	68	76	82	27	38	29	9
Zr	178	195	127	195	158	268	202	31	37	41	25
Ag	0.09	0.06	0.04	0.07	0.08	0.1	nd	0.01	0.03	0.02	0.01
Bi	0.22	0.19	0.14	0.65	0.31	0.45	nd	0.19	0.12	0.12	0.04
Sb	0.25	0.45	0.14	2.4	9.5	13.6	nd	3.2	1.3	3.2	2.5
Sr/Ba	0.76	0.62	0.50	3.34	1.08	1.25	0.41	1.99	4.24	2.29	2.33

Oxides and loss-on-ignition (LOI) are in wt.%; trace elements are in ppm. All iron is calculated as ferric. nd=not determined.

The alteration halo is apparently wider in the drill core than in historic mine workings accessible at the surface (Fig. 5). In these surface exposures, the siliceous mineralised zone that constituted the principal target for mining is only 20–30 cm thick. This zone consisted of sheared, brecciated, and variably silicified rock with a core of quartz veins and silicified breccias. Minor orange iron oxyhydroxide staining of host rocks near the fault zones attest to the presence of ankerite that has been weathered. Deeper workings are no longer accessible, but historic records suggest that they followed the quartz-rich zone along the Bullendale Fault (Fig. 3; Williams, 1974; Begbie and Craw, 2006).

5. Structural controls on alteration

5.1. Shears

Flexural slip deformation during development of the kink folds in fissile schist has resulted in formation of foliation-parallel shears throughout the cored sections. These shears are irregularly developed through the sections, with some zones having shears spaced less than 1 cm apart (Fig. 6A and B). This close spacing of shears persists locally on the 10 to 50 cm scale, and these zones are separated by up to 5 m of essentially unsheared rock. Locally, shears are so strongly developed that they dominate the rock fabric, and the rock breaks along strongly slickensided shiny surfaces (Fig. 6A). Shears occur mainly in micaceous laminae (Fig. 6A and B), but more strongly deformed zones have anastomosing shears that step across quartz-albite laminae. Shears parallel to the foliation on the limbs of kink folds have propagated along the fold axial surface of tighter parts of the fold hinges (Fig. 2A). More intense deformation with this geometry has resulted in through-going fold axial surface shears, along which there has been displacement on the millimetre to centimeter scale (Fig. 2B). Similar processes have reactivated the micaceous hinge zone and limb of an isoclinal synmetamorphic fold in Fig. 6A.

The shears appear as thin black seams (<0.1 mm wide) in hand specimen and thin section (Figs. 2A and B; 6A and B). The shear zones consist primarily of muscovite that has been cataclastically deformed, with minor recrystallisation. This fine-grained muscovite is interspersed with rutile that has formed from decomposition of metamorphic titanite. Shear-related rutile is finer-grained than the metamorphic titanite, and forms irregular composite grains elongate parallel to the shear host. Metamorphic chlorite has been recrystallised with hydrothermal muscovite in shears distant from the Bullendale Fault (Fig. 2A). Chlorite is partially (Fig. 2B) or wholly (Fig. 7A and B) replaced by hydrothermal ankerite within the Bullendale alteration halo (Figs. 3 and 4).

Pyrite, arsenopyrite, and rare chalcopyrite, occur along many of the shears in the alteration halo (Fig. 7A–D), and some of these sulphides contain micron-scale native gold (Fig. 8). Muscovite has recrystallised with, and around, some sulphide grains (Fig. 7D). Sulphide grains in shears are commonly elongate, ragged and deformed (Fig. 7B).

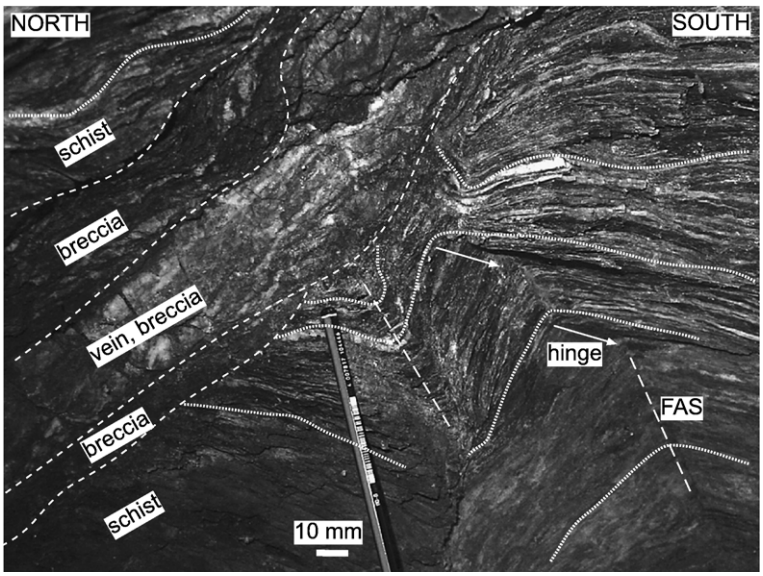

Fig. 5. Photograph of the Bullendale Fault Zone exposed near-surface in historic workings. Segregated schist foliation (heavy white dotted lines) is kink-folded, with fold axial surfaces (FAS) indicated by long-dashed white lines. Folds have been truncated by zones of breccias and veins (outlined by short-dashed white lines). The core vein and breccia zone has been silicified and then refaulted with sulphide addition, to form dark lines at centre top.

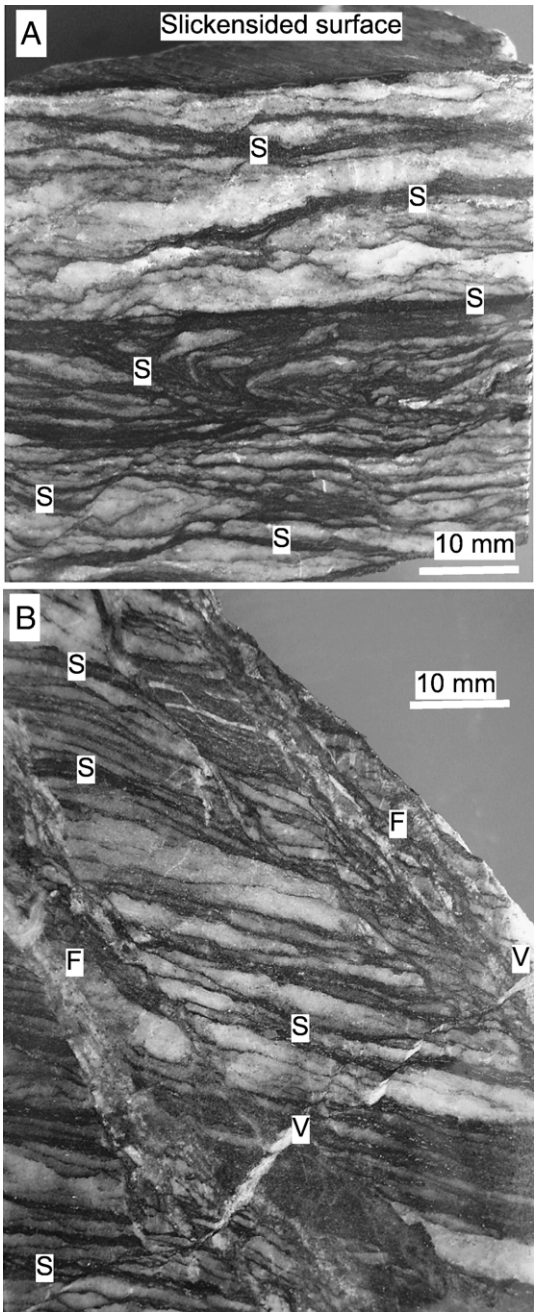

Fig. 6. Photographs of structures in core from drill core. A. Micaceous laminae in segregated schist have been sheared parallel to foliation (S) during flexural-slip folding, resulting in spaced black altered seams. One such seam has been reactivated by later faulting to form a slickensided surface (top). Location: BD2, 133.0 m. B. Segregated schist foliation with dark shears (S) have been cut by normal fault zones (F) that contain quartz±albite veins and silicified breccias, and have ankeritic alteration of breccias and fault margins. The faults have been cut by late stage veinlets (V). Location: BD1, 67.3 m.

Deformed sulphides contribute to the dark colour of shears. Some sulphides have euhedral shapes, as progressive shearing has bypassed them (Fig. 7D). Shears in the muscovite-rich layers are commonly accompanied by fracture arrays in the adjacent quartz-albite laminae, at the millimetre to centimeter scales. These fracture arrays are filled with ankerite veinlets in the Bullendale alteration halo (Fig. 7A and B). Pyrite and arsenopyrite accompany this fracture-filling ankerite, resulting in disseminated sulphide textures locally (Fig. 7C). Some recrystallisation of quartz, with minor ankerite impregnation, has occurred along fractures in quartz-albite laminae in the alteration halo as well (Fig. 2B).

Kaolinite (X-ray diffraction identification) is intergrown with, and overprints, cataclastically deformed and partially recrystallised muscovite in the more sulphidic zones near the Bullendale Fault Zone (Fig. 7D). The kaolinite is typically undeformed when it occurs in muscovite-rich shears. Kaolinite has also grown in strain-shadows beside sulphide grains (Fig. 7D) where it is undeformed also.

5.2. Faults

Foliation-parallel shears have been overprinted by normal faults at a high angle to the foliation (Fig. 6B). These faults occur sporadically through the alteration halo, with approximately 30–50 cm spacing. An isolated but well-defined fault occurs about 150 m structurally above the alteration halo as well (Fig. 3). The narrowest fault zones are 1–2 mm wide, but most are 1–2 cm wide. The Bullendale Fault Zone itself consists of several superimposed metre-scale faults (Fig. 5).

Faults were clearly extensional along most of their length, with dip-slip displacements of millimetres to centimetres (Fig. 6B). Offset across the main Bullendale Fault Zone is not known. Extensional cavities along faults have been filled with brecciated host rock that has been cemented by quartz, albite, and ankerite vein material. Kaolinite occurs within breccia matrix, interspersed with cementing quartz and ankerite. Sulphides (pyrite and arsenopyrite) form seams parallel to the fault zone, and scattered grains are disseminated through silicified breccias. Gold is closely associated with these sulphides, mainly as encapsulated grains. Sulphidic silicified breccias have been sheared and deformed along well-defined fault planes, resulting in hard slickensided surfaces. Likewise, quartz and albite veins have been locally brecciated and recemented by quartz. Vein albite is generally coarse grained (2–3 mm), and coarsely twinned, in contrast to untwinned metamorphic albite in adjacent foliation-parallel laminae. Some vein albite twin planes have been bent and/or fractured by post-depositional deformation.

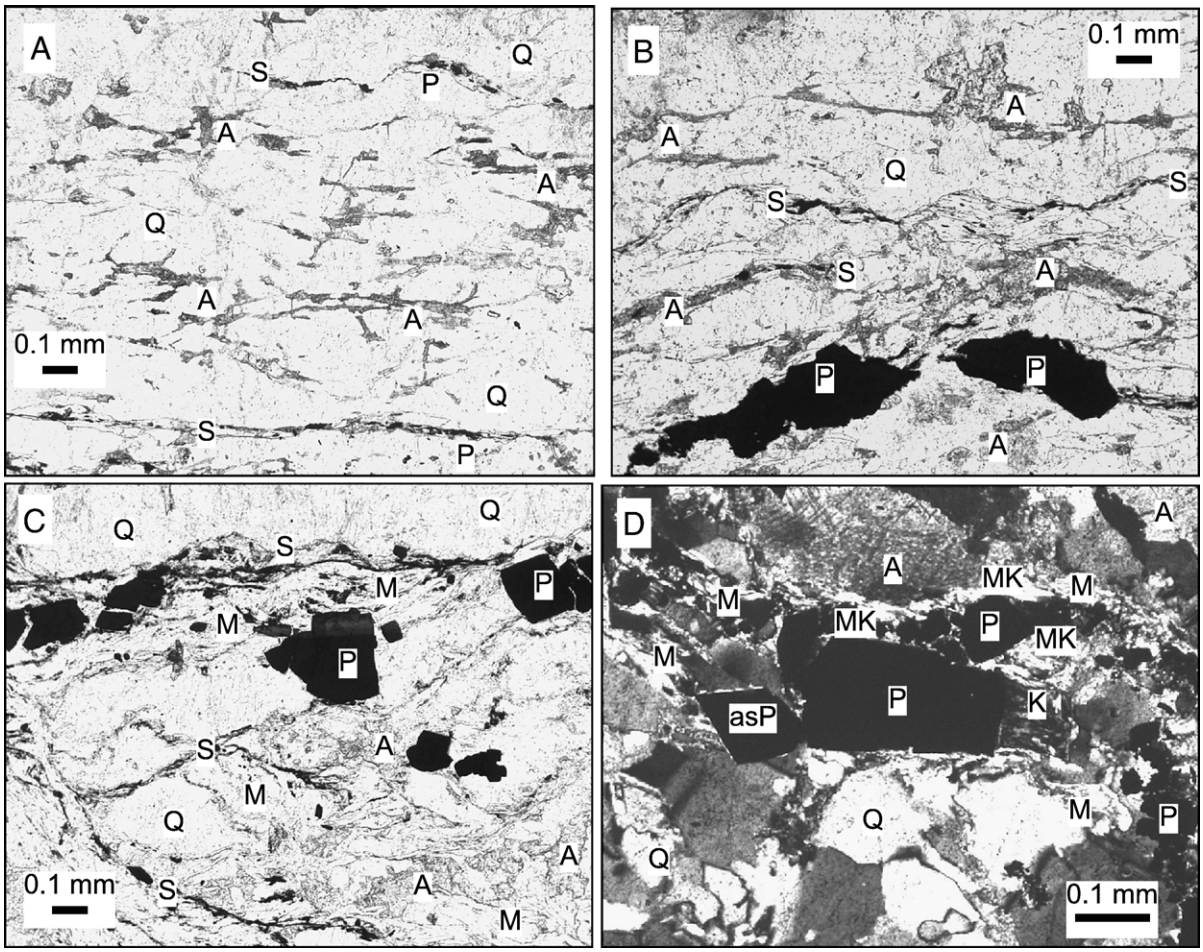

Fig. 7. Photomicrographs of variably altered schist from the Bullendale alteration halo. A–C are transmitted light images; D is a crossed-polar image. A. Quartz-albite segregation (white, Q) with narrow sheared micaceous laminae (S, top and bottom) containing streaks of fine-grained hydrothermal pyrite (black, P). The quartz-rich segregation has been microfractured and impregnated with a network of ankerite veinlets (A, grey). Location: BD1, 303 m. B. More micaceous rock than in A, with more numerous pyritic shears and coarser grained hydrothermal pyrite and arsenopyrite (black, P). Ankerite (A) in micaceous laminae has replaced chlorite. Location: BD1, 303 m. C. Strongly mineralised mica-rich schist with pyritic shears, disseminated pyrite and arsenopyrite (P, black), and disseminated ankerite (A) replacing chlorite. Location: BD1, 323 m. D. Strongly mineralised and sheared mainly micaceous schist with black pyrite (P) and arsenopyrite (asP). Sulphide grains are surrounded by hydrothermal muscovite (M), kaolinite (K), and mixed muscovite and kaolinite (MK), with coarse ankerite (A) veins and replacement patches. Location: BD2, 261 m.

5.3. Post-mineralisation veins

A set of thin (0.1–1 mm) extensional veinlets cuts across mineralised and unmineralised structures, at a high angle to the foliation (Fig. 6B). These veinlets are commonly discontinuous on the centimetre scale (Fig. 6B), but some wider veins cut continuously across the core. The veinlets are irregularly spaced down the core, but are typically 10–30 cm apart. The principal minerals are chlorite and calcite, with quartz in some veinlets. Pyrite is rare, and occurs with chlorite. No gold has been detected in this generation of veins, either visually or via assays.

6. Mineralogy and geochemistry of the alteration halo

6.1. Host rock composition

Metamorphic mineralogy of host rocks and minerals formed during subsequent generations of hydrothermal alteration are summarised in Fig. 9. The host schists have highly variable compositions at the scale of sampling in this study, principally because of the strong metamorphic segregation on the millimeter to centimetre scale. Host rock analyses reflect this strong segregation (Table 1; Figs. 10 and 11). Higher proportions of micaceous laminae in samples result in higher magnesium and water

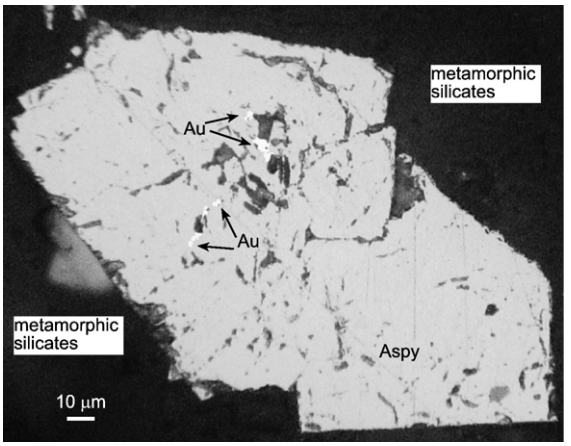

Fig. 8. Incident light photomicrograph of an arsenopyrite (Aspy; grey) grain in micaceous schist (drillhole BD2, 261 m; Fig. 7D), showing included micron-scale gold grains (Au, white).

contents (Fig. 10A and B) because chlorite occurs mainly in those micaceous laminae. The different proportions of these segregations in samples results in an inverse correlation (Fig. 10C) between sodium contents (mainly reflecting albite in segregation veins) and potassium contents (reflecting muscovite in micaceous laminae). The silica contents of the host schists (Fig. 11A) range from <60 wt.% (mica-rich samples) to >70 wt.% (samples rich in quartz-albite segregations). Trace element contents of the host schist samples are also highly variable because of the metamorphic segregation (e.g., Sr, Ba; Fig. 11E, F). Hence, direct comparison of compositions of unaltered and hydrothermally altered rocks is difficult, and can be done only in the context of the broad range of host rock compositions (Figs. 10 and 11). We focus here primarily on the observable changes in mineralogy associated with alteration (Fig. 9), and relate these changes to variations in bulk rock compositions using measured mineral compositions.

6.2. Ankerite

Ankerite is the most prominent hydrothermal mineral in the alteration halo, as described in the previous sections. Ankerite alteration and vein formation was initiated during kink folding (Craw et al., 2006) and persists through the shears and faults (Fig. 9). The ankerite is ferroan dolomite with generally uniform composition, containing 11 to 23 mol% siderite component. The ankerite alteration has resulted in a substantial increase in carbonate content of the rocks, as indicated by a general increase of ca. 2 wt.% loss-on-ignition (LOI) of altered rocks (Figs. 10A and 11A). However, LOI is highly variable within the most mineralised zones (e.g., base of BD 2; Fig. 12A). Despite the widespread ankerite formation, the MgO contents of the rocks (typically 1–2 wt. %) have changed little compared to unaltered rocks, apart from two samples that are clearly anomalously ankerite-rich (Fig. 10A).

Unaltered rocks have near-constant iron/magnesium ratios, with molar Fe/(Fe+Mg) of ca. 0.6 (Fig. 10B). Likewise, altered and silicified rocks have essentially

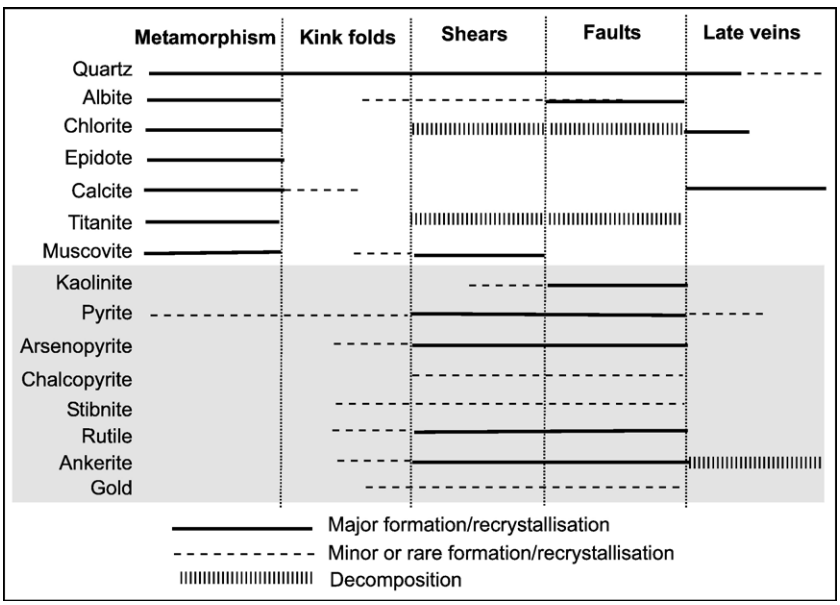

Fig. 9. Summary paragenesis diagram, showing mineral assemblages during different structural generations in the Bullendale alteration halo. Stibnite has not been detected in the halo, but occurs in nearby alteration zones.

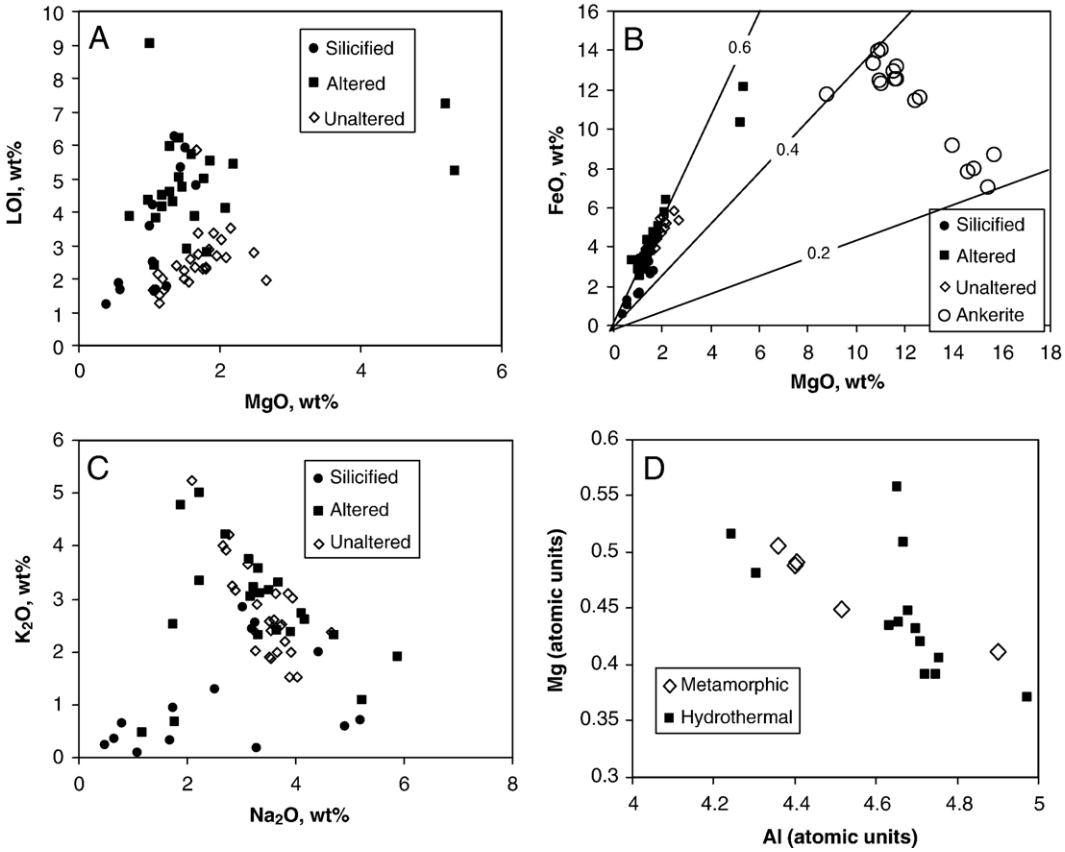

Fig. 10. A. Magnesium contents and loss-on-ignition (LOI) of unaltered, altered, and silicified rocks from the Bullendale alteration halo. B. Magnesium and iron contents of Bullendale alteration halo rocks (as for A), compared to the composition of hydrothermal ankerite. Lines show Fe/(Fe+Mg) ratios. XRF analyses have been recalculated to FeO to facilitate comparison. C. Sodium and potassium contents of Bullendale alteration halo rocks (as for A). D. Comparison of Al and Mg contents of metamorphic and hydrothermal muscovites from the Bullendale alteration halo.

the same ratios as the unaltered rocks, except for minor deviations to lower iron/magnesium ratio of the two samples with elevated MgO (Fig. 10A and B). In contrast, the ankerite compositions, recalculated to plot on Fig. 10B, have distinctly lower iron/magnesium ratios [molar Fe/(Fe+Mg)=0.2 to 0.4].

6.3. Muscovite and albite

Muscovite is a major component of unaltered rocks, and muscovite-rich laminae have controlled much of the early stages of alteration via shears (Figs. 2, 6, 7 and 9). Some of this deformed muscovite recrystallised in shears, but not in the later faults (Figs. 7 and 9). However, there is no evidence, either petrographic (such as replacement of other silicates) or geochemical, for crystallisation of new muscovite in the rocks during alteration. Altered rocks have potassium contents in essentially the same range as unaltered rocks, although both altered and unaltered rocks are highly variable (Fig. 10C).

Recrystallised muscovite in shears in the altered rocks is fine-grained (ca. 20 μm) and commonly intimately intergrown with other minerals. Hence, microprobe analysis of this material is difficult. Comparison of metamorphic and hydrothermal muscovite compositions suggests that the hydrothermal muscovite is less phengitic than the metamorphic muscovite, with generally higher Al and lower Mg (and Fe) in the hydrothermal micas (Fig. 10D). There is considerable overlap in the data sets (Fig. 10D), which is probably at least partly a result of misidentification of grains of the different generations of mica during analysis. However, the differences in muscovite compositions are small (Fig. 10D), and there is no discernible elevation of bulk rock aluminium content, and associated depletion of magnesium content, of altered rocks (Table 1).

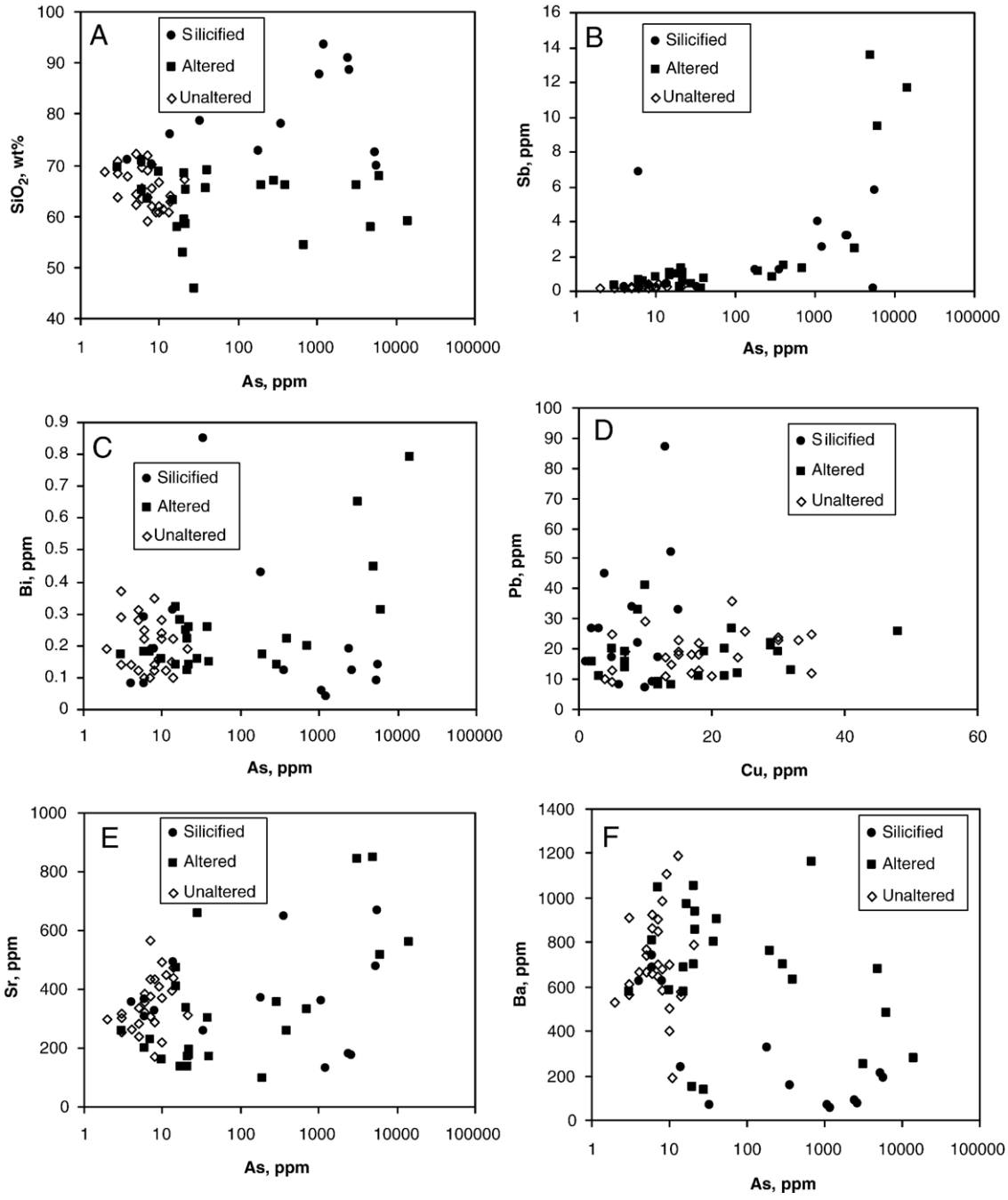

Fig. 11. A–D Trace metal/metalloid concentrations in rocks from the Bullendale alteration halo. E, F. Variations of Sr and Ba contents with As concentrations in the Bullendale alteration halo.

The principal geochemical trend in Fig. 10C, of both altered and unaltered rocks, is an inverse relationship between sodium and potassium contents, reflecting differing proportions of albite and muscovite respectively. Several altered and silicified rocks at the high sodium, low potassium end of this trend are outside the range defined by unaltered rocks. These high sodium rocks contain abundant hydrothermal albite in fault-hosted veins, in addition to foliation-parallel metamorphic albite. Both albite generations are pure end-member albite with no detectable Ca or K.

Most silicified rocks fall off the inverse Na_2O vs K_2O trend, and lie on a trend towards very low (near zero) potassium and sodium (Figs. 10C and 12A). The

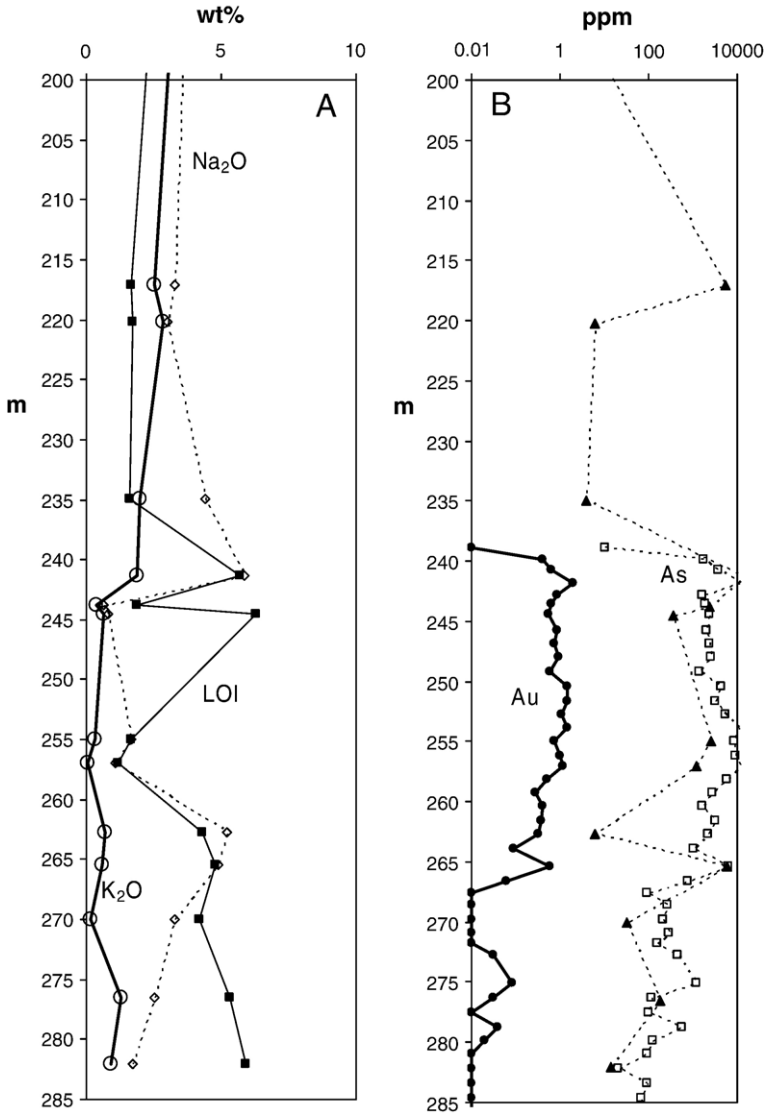

Fig. 12. Chemical variations of key parameters through the lower portion of drillhole BD 2. A. Variations in Na_2O (dotted line and open diamonds), K_2O (light line and filled squares) and LOI (heavy line and open circles) with depth. B. Variations of Au (heavy line and filled circles) and As (dotted lines) with depth. Two sets of data are provided for As: XRF (filled triangles) and AA (open squares).

addition of hydrothermal quartz to these rocks has resulted in dilution of pre-alteration sodium and potassium contents. Likewise, the two high MgO (ankerite-rich) altered samples in Fig. 10A and B also have lowered (diluted) sodium and potassium contents (Fig. 10C).

6.4. Sulphides

The addition of arsenic to form arsenopyrite along shears and in faults is second only to ankerite in importance in the alteration halo. The resultant arsenic geochemical signature is highly distinctive (Figs. 3 and 12B). Arsenic is strongly enriched in both altered (ankeritic) and silicified rocks in the alteration halo (Fig. 11A). There is a general increase in arsenic with increasing silica contents of silicified rocks (Fig. 11A), attesting to the high arsenopyrite content of the siliceous breccias in faults. In contrast, the silica content of altered schist either remained constant or was lowered (diluted) during arsenopyrite addition (Fig. 11A).

Arsenopyrite is unzoned, and has uniform composition of 29.5–31.5 mole% As (microprobe analysis). Antimony is not detectable in the arsenopyrite via

microprobe analysis. However, the positive correlation (linear $R^2=0.73$) between bulk rock Sb and As for altered rocks (Fig. 11B) suggests that Sb is in solid solution or micro-inclusions in the arsenopyrite, albeit at low concentrations. Similarly, the minor bismuth enrichment in altered rocks is generally correlated (linear $R^2=0.73$) with arsenic (Fig. 11C), so Bi may be present in solid solution or micro-inclusions in arsenopyrite as well. Gold is closely associated with arsenopyrite (Fig. 12B), either as inclusions (Fig. 8) or disseminated through nearby hydrothermally altered schist.

Pyrite occurs with arsenopyrite in shears (Fig. 7D) and faults throughout the alteration halo. Pyrite also occurs without arsenopyrite on many shears, particularly near the edge of the main alteration halo (Fig. 7A–C), and beyond that halo where shears are only incipiently developed. Distinction between structurally-controlled hydrothermal pyrite and scattered metamorphic pyrite is difficult in weakly folded rocks (Fig. 2A), and neither pyrite generations have As contents detectable by microprobe (>0.3 wt.%). Despite the presence of abundant pyrite in many altered rocks, there is no evidence for iron enrichment in these rocks compared to unaltered rocks (Fig. 10B). Pyrite is essentially a replacement mineral arising from addition of sulphur to iron-bearing rock (cf. Böhlke, 1988). This added sulphur contributes to the elevated LOI of altered rocks (Figs. 10A and 12A). The rock with the highest LOI, and low MgO (Fig. 10A) is particularly pyrite-rich.

Rare chalcopyrite occurs as part of the original metamorphic mineral assemblage in rocks distant (>100 m) from the mineralised zone, scattered through micaceous laminae that have not been reactivated by later deformation. Chalcopyrite occurs also as a minor hydrothermal mineral, locally accompanying hydrothermal pyrite and arsenopyrite. Hydrothermal chalcopyrite also occurs sporadically with ankerite in microveinlets cutting across quartz-albite laminae. Apart from one altered sample, there is no evidence for copper enrichment during alteration (Fig. 11D). Likewise, there is no evidence for lead or zinc enrichment, either petrographically or geochemically (Table 1; Fig. 11D).

6.5. Lithophile trace elements

There were no apparent enrichments or depletions of most trace element concentrations during alteration (Table 1). Strontium and barium appear to be exceptions (Table 1; Fig. 11E and F). Several of the most altered rocks have Sr concentrations of >600 ppm, compared to unaltered rocks that have Sr concentrations of 200–500 ppm (Fig. 11E). There is a crude positive correlation (linear $R^2=0.33$) between As and Sr concentrations in altered rocks (Fig. 11E). Even the silicified rocks, in which most elements have been diluted by silica addition (e.g. Fig. 10C) have Sr concentrations equivalent to, or higher than, unaltered host rocks. In contrast, barium concentrations of some altered rocks appear to have been depleted compared to unaltered rocks (Fig. 11F).

7. Discussion

7.1. Geochemical signature of alteration

For most of the analysed elements, the variation of host rock compositions is as great, or greater than, differences between unaltered and altered rocks (Table 1; Figs. 10 and 11). There have been detectable additions of As (and probably Sb and Bi), S, CO_2, Sr (Figs. 10A and 11A, B, E), and gold (Fig. 12B). Barium has apparently been depleted. The overall style of alteration, dominated by carbonation and sulphidation, resembles some of those described from other goldfields by Kishida and Kerrich (1987), Böhlke (1988), Gao and Kwak (1997), Eilu and Mikucki (1998) and McCuaig and Kerrich (1998). However, unlike most of these examples, the Bullendale alteration has no evidence for addition or depletion of alkalis (Fig. 10C) or aluminium. Hence, calculated parameters such as "sericitisation indices" (e.g., Kishida and Kerrich, 1987; Eilu and Mikucki, 1998) do not help to define Bullendale alteration. The carbonation at Bullendale is most distinctive, and "carbonation indices" (e.g., Kishida and Kerrich, 1987; Eilu and Mikucki, 1998) could be used as indicators of the extent of the alteration halo. However, occurrences of variable amounts of metamorphic calcite, gold-related ankerite, and post-mineralisation calcite in the same rocks render these indices less useful. LOI, a less specific but simpler parameter determined in this study, is more useful as it combines added S and CO_2 components plus the extra hydration associated with hydrothermal kaolinite (Figs. 10A and 12A). Likewise, addition of Sr and depletion of Ba during Bullendale alteration could be used to define an alteration halo, with, for example, a Sr/Ba ratio>1 implying significant alteration. However, there is wide scatter of both Ba and Sr compositions (Fig. 11E and F), and some altered rocks have Sr/Ba of ca. 0.2–0.4, lower than typical host rocks (Table 1). Only the silicified rocks have generally high Sr/Ba of 2–5 (Table 1).

The geochemical indicators of alteration described in the previous paragraph may point to hydrothermal alteration, but they are of little value as vectors towards

the most mineralised rocks (cf. Kishida and Kerrich, 1987; Gao and Kwak, 1997; Eilu and Mikucki, 1998). This lack of alteration directionality is a result of the abundant small-scale structures that have controlled the alteration (Figs. 2, 6 and 7). Alteration has occurred along these structures, and unaltered rock is preserved within a few centimetres on either side of many of these structures. Hence, it is the increasing frequency of shears and faults that are the best indicators of the alteration halo, combined with the alteration minerals that are readily observed in hand specimen within those structures.

7.2. Alteration reactions

The paragenetic sequence inferred from structural observations and petrography (Fig. 9) shows that there are two principal hydrothermal mineral assemblages developed in the alteration halo. These assemblages developed sequentially during evolution of structural permeability in the alteration halo. The principal differences are that the earliest assemblage, formed in the latter stages of kink fold development and shear formation, involves recrystallised muscovite, whereas a subsequent assemblage in faults has kaolinite replacing muscovite in altered schist, and deposition of albite in veins (Fig. 9). Other hydrothermal minerals, such as ankerite and sulphides, are found throughout the structures that have controlled fluid flow. Likewise, chlorite and titanite decomposition reactions occurred throughout the alteration sequence (Fig. 9) although most of these metamorphic minerals reacted in the earlier alteration stages. Carbonate minerals accompany all stages of alteration, attesting to a dissolved carbonate component in the hydrothermal fluid. This is in accord with the presence of immiscible CO_2-bearing fluid inclusions in quartz veins, although the CO_2 content of the fluid is inferred to be low (Craw et al., 1991).

Hydrothermal ankerite has distinctly lower Fe/(Fe+Mg) ratios than that of the host rocks (Fig. 10B), so excess iron released from hydrothermal alteration of chlorite and muscovite (the principal iron-bearing minerals) was available for formation of pyrite. Epidote decomposition may also have contributed some iron for pyrite formation. Pyrite formation from iron released during carbonate formation in high Fe/(Fe+Mg) rocks is reputedly a key feature facilitating gold deposition during alteration (Böhlke, 1988).

7.3. Mineral zonation

There is no evidence for spatial mineral zonation in the Bullendale alteration halo, although some zones are richer in some hydrothermal minerals (e.g., ankerite, quartz) than others (Figs. 3 and 4). Rather, hydrothermal mineral distribution is controlled principally by the hosting structures. Hence, the same suite of alteration minerals occurs in shears or faults at the edge of the alteration zone as in the main Bullendale Fault Zone

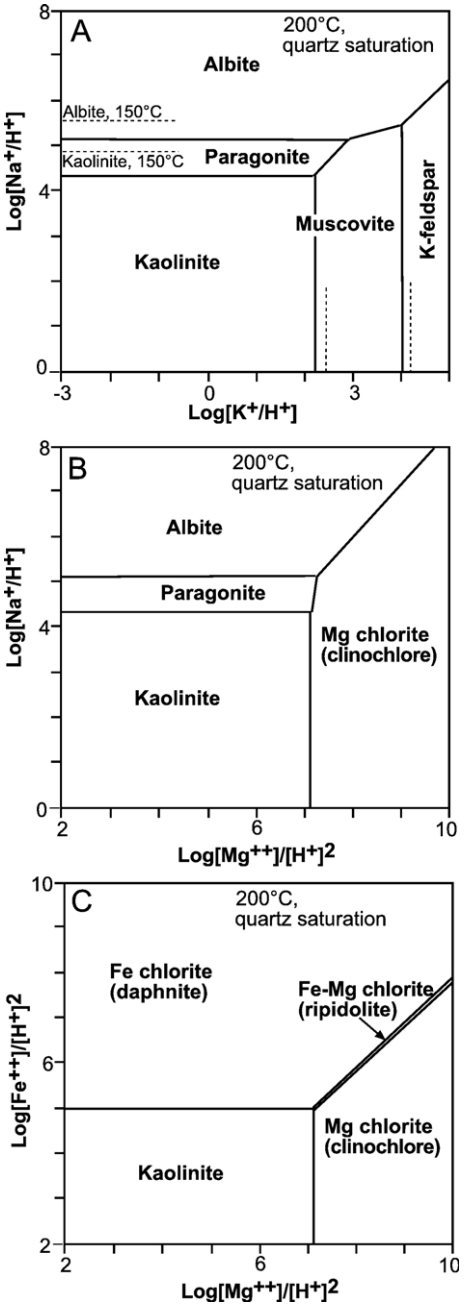

Fig. 13. Model activity-activity diagrams showing the geochemical relationships among minerals in the Bullendale alteration halo. Diagrams were drawn using program ACT2, part of the Geochemists Workbench package (Bethke, 2005).

(Fig. 3). Likewise, geochemical effects of alteration are indistinguishable between the edge and the centre of the Bullendale alteration halo. The scale of development of alteration minerals is related directly to the scale of development of the host structures. Small faults up to 150 m from the main Bullendale Fault Zone have alteration extending only millimetres or, at most, centimetres from the hosting structures, but can include evidence for the same hydrothermal reactions and gold mineralisation as the core of the alteration halo. The more permeable Bullendale Fault Zone is the most mineralised zone because it was the focus for fluid flow and locus for pronounced and repeated deformation and associated alteration, and there is mappable zonation in intensity of alteration types around this fault zone (Figs. 3, 4 and 5).

Despite the poor spatial mineral zonation, there were some temporal changes in alteration mineralogy. The most prominent of these is the change from minor hydrothermal muscovite formation (mainly in early shears) to kaolinite formation (mainly associated with later faults; Fig. 7D, 9). This change was accompanied, approximately contemporaneously, by formation of vein albite in later faults (Fig. 9). Destabilisation of muscovite to form kaolinite or albite can be depicted on an activity-activity diagram (Fig. 13A). Paragonite is depicted in these diagrams as a separate mineral, but is a solid solution component of muscovite in the alteration halo. Only small changes in fluid chemical parameters (sodium or potassium activity, pH) and/or temperature are required to effect the observed changes in mineralogy. Likewise, small changes in magnesium and iron activities result in stabilisation of kaolinite or albite with respect to chlorite (Fig. 13B and C). The details of these varying parameters are beyond the scope of this study, but these diagrams serve to demonstrate that this geochemical system is delicately poised, and the obvious changes in alteration mineralogy do not necessarily signify major changes in hydrothermal processes. The reappearance of chlorite in late stage veins (Figs. 6B and 9) is also probably a consequence of either temperature change and/or minor change in solution composition (Fig. 13B and C).

8. Conclusions

The Bullendale alteration halo involves hydrothermally altered rocks up to 150 m across strike from a major mineralised fault zone. The most pronounced alteration zone is ca. 50 m wide, around a narrow (ca. 5 m) set of quartz veins that were mined historically. The hydrothermal alteration was strongly controlled by small-scale (microns to metres) structures that developed during regional compressional deformation of highly fissile segregated schist. Microshears developed with increasing deformation into anastomosing subparallel sets that locally cut through kink fold hinges. Later, but related, normal fault zones (centimetre to metre scale) cut across folds and early-formed microshears.

Hydrothermal alteration in and adjacent to the microshears and faults is dominated by direct replacement of metamorphic chlorite by ankerite in micaceous laminae in the host schist. Ankerite also filled microfractures in more competent intervening quartz-albite metamorphic segregations. Recrystallisation of metamorphic muscovite to more aluminous muscovite occurred within micaceous laminae, and at a later stage, muscovite was altered to kaolinite. The alteration reactions released Fe, which combined with added S and As to form pyrite and arsenopyrite, principally in micaceous laminae. Gold accompanies these sulphide minerals. The most intensely altered fault zones have abundant quartz veins, silicified breccias, and silicified wall rocks, and these all contain sulphides and gold. Albite is a common vein mineral in these intensely altered rocks. Intensity of alteration can be mapped at the metre scale around the main Bullendale Fault Zone, but similar features are seen at smaller scales around minor structures farther removed from the fault zone.

The ankeritic impregnation and associated formation of sulphide minerals has resulted in an increase in rock volatile content (loss-on-ignition, LOI) from ca. 3 wt.% to ca. 6 wt.%. Addition of As is highly distinctive, and As levels up to 10,000 ppm occur in the most hydrothermally altered rocks. Minor Sb enrichment (up to 14 ppm) accompanied this arsenic enrichment. Strontium is enriched, and Ba depleted, in many of the altered rocks, although this is not consistent. The most hydrothermally altered rocks have Sr/Ba of ca. 3–5, compared to <1 in host rocks. The geochemical signature of the mineralisation is subtle, and the alteration mineralogy is more useful as an indicator of hydrothermal processes. The alteration halo enlarges the exploration target of this deposit by at least an order of magnitude, and this style of alteration is a common phenomenon around orogenic (mesothermal) deposits of this type.

Acknowledgements

This study was financed by the NZ Foundation for Research, Science and Technology and University of Otago. Core access was provided by the NZ Ministry of Economic Development (Crown Minerals). Discussions with R.H. Sibson and R.J. Norris helped us develop ideas expressed herein. Technical assistance from Adrien Dever, John Williams, Lorraine Paterson, and

Damian Walls was extremely helpful in conducting the study. Thorough reviews by F. Bierlein and an anonymous referee substantially improved the presentation of the manuscript.

References

Begbie, M., Craw, D., 2006. Gold mineralisation in the Shotover–Macetown region, NW Otago, New Zealand. In: Christie, A.B., Brathwaite, R. (Eds.), Geology and Exploration of New Zealand Mineral Deposits. Australas. Inst. Min. Metall. Monogr., vol. 25, pp. 299–304.

Bethke, C.M., 2005. Geochemists Workbench, Release 6.0, Hydrogeology Program. University of Illinois, USA.

Bierlein, F.P., Crowe, D., 2000. Phanerozoic orogenic lode gold deposits. In: Hagemann, S.G., Brown, P.E. (Eds.), Gold in 2000. Rev. Econ. Geol., vol. 13, pp. 103–140.

Bierlein, F.P., Maher, S., 2001. Orogenic disseminated gold in Phanerozoic fold belts: examples from Victoria, Australia, and elsewhere. Ore Geol. Rev. 18, 113–148.

Bierlein, F.P., Arne, D.C., McKnight, S., Lu, J., Reeves, S., Besanko, J., Marek, J., Cooke, D., 2000. Wall-rock petrology and geochemistry in alteration halos associated with mesothermal gold mineralization, central Victoria, Australia. Econ. Geol. 95, 283–312.

Böhlke, J.K., 1988. Carbonate-sulfide equilibria and "stratabound" disseminated epigenetic gold mineralization: a proposal based on examples from Alleghany, California, USA. Appl. Geochem. 3, 499–516.

Christie, A.B., Brathwaite, R.L., 2003. Hydrothermal alteration in meta sedimentary rock-hosted orogenic gold deposits, Reefton goldfield, South Island, New Zealand. Miner. Deposita 38, 87–107.

Cooper, A.F., 1986. A carbonatitic lamprophyre dike swarm from the Southern Alps, Otago and Westland. Cenozoic volcanism in New Zealand. R. Soc. N.Z., Bull. 23, 313–336.

Cooper, A.F., Barreiro, B.A., Kimbrough, D.L., Mattinson, J.M., 1987. Lamprophyre dike intrusion and the age of the Alpine fault, New Zealand. Geology 15, 941–944.

Cox, S.F., Wall, V.J., Etheridge, M.A., Potter, T.F., 1991. Deformation and metamorphic processes in the formation of mesothermal vein-hosted gold deposits: examples from the Lachlan Fold Belt in central Victoria, Australia. Ore Geol. Rev. 6, 391–423.

Craw, D., 1985. Structure of the schists in the Mt Aspiring region, northwestern Otago. N.Z. J. Geol. Geophys. 28, 55–75.

Craw, D., 1989. Shallow-level, late-stage gold mineralisation in Sawyers Creek, Shotover valley, North West Otago, New Zealand. NZ J. Geol. Geophys. 32, 375–384.

Craw, D., 2002. Geochemistry of late metamorphic hydrothermal alteration and graphitisation of host rock, Macraes gold mine, Otago Schist, New Zealand. Chem. Geol. 191, 257–275.

Craw, D., Norris, R.J., 1991. Metamorphogenic Au–W veins and regional tectonics: mineralisation throughout the uplift history of the Haast Schist, New Zealand. N.Z. J. Geol Geophys. 34, 373–383.

Craw, D., Reay, A., Johnstone, R.D., 1991. Hydrothermal alteration geochemistry of Nugget gold vein system, Shotover valley, northwest Otago, New Zealand. N.Z. J. Geol. Geophys. 34, 419–427.

Craw, D., Windle, S.J., Angus, P.V., 1999. Gold mineralization without quartz veins in a ductile-brittle shear zone, Macraes Mine, Otago Schist, New Zealand. Miner. Deposita 34, 382–394.

Craw, D., Begbie, M., MacKenzie, D., 2006. Structural controls on Tertiary orogenic gold mineralization during initiation of a mountain belt, New Zealand. Miner. Depos. 41, 645–659.

Eilu, P., Mikucki, E.J., 1998. Alteration and primary geochemical dispersion associated with the Bulletin lode-gold deposit, Wiluna, Western Australia. J. Geochem. Explor. 63, 73–103.

Gao, Z.L., Kwak, T.A.P., 1997. The geochemistry of wall rock alteration in turbidite-hosted gold vein deposits, central Victoria. J. Geochem. Explor. 59, 259–274.

Goldfarb, R.J., Baker, T., Dube, B., Groves, D.I., Hart, C.J., Gosselin, P., 2005. Distribution, character and genesis of gold deposits in metamorphic terranes. In: Hedenquist, J.W., Thompson, J.F.H., Goldfarb, R.J., Richards, J.P. (Eds.), Econ Geol. 100th Anniv. Vol: 407–450.

Gray, D.R., Foster, D.A., 2004. $^{40}Ar/^{39}Ar$ thermochronologic constraints on deformation, metamorphism and cooling/exhumation of a Mesozoic accretionary wedge, Otago Schist, New Zealand. Tectonophysics 385, 181–210.

Gray, D.R., Gregory, R.T., Durney, D.W., 1991. Rock-buffered fluid-rock interaction in deformed quartz-rich turbidite sequences, eastern Australia. J. Geophys. Res. 96, 19681–19704.

Kishida, A., Kerrich, R., 1987. Hydrothermal alteration zoning and gold concentration at the Kerr-Addison Archean lode gold deposit, Kirkland Lake, Ontario. Econ. Geol. 82, 649–690.

Kontak, D.J., Smith, P.K., Kerrich, R., Williams, P.F., 1990. Integrated model for Meguma Group lode gold deposits. Geology 18, 238–242.

McCuaig, T.C., Kerrich, R., 1998. P-T-t-deformation-fluid characteristics of lode gold deposits: evidence from alteration systematics. Ore Geol. Rev. 12, 381–453.

Mitchell, M., Maw, L., Angus, P.V., Craw, D., 2006. The Macraes gold deposit in east Otago. Geology and exploration of New Zealand mineral deposits. Australas. Inst. Min.. Metall. Monogr. 25, 313–318.

Mortimer, N., 1993. Geological map of the Otago Schist and adjacent rocks, scale 1:500,000., Map 7. Lower Hutt, NZ, Inst. Geol. Nuclear Sci. Ltd.

Phillips, G.N., Powell, R., 1993. Links between gold provinces. Econ. Geol. 88, 1084–1098.

Sibson, R.H., Robert, F., Poulsen, K.H., 1988. High-angle reverse faults, fluid-pressure cycling, and mesothermal gold–quartz deposits. Geology 16, 551–555.

Turnbull, I.M., 2000. Geology of the Wakatipu area. 1:250 000 geological map 18. 1 sheet+ 72 p. Lower Hutt, NZ, Inst. Geol. Nuclear Sci. Ltd.

Turnbull, I.M., Barry, J.M., Carter, R.M., Norris, R.J., 1975. The Bobs Cove beds and their relationship to the Moonlight Fault Zone. J. Royal Soc. N.Z. 5, 355–394.

Turnbull, I.M., Mortimer, N., Craw, D., 2001. Textural zones in the Haast Schist: a reappraisal. N.Z. J. Geol. Geophys. 44, 171–183.

Williams, G.J., 1974. Economic geology of New Zealand. Australas. Inst. Min. Metall. Monogr. 4.

Witt, W.K., Vanderhor, F., 1998. Diversity within a unified model for Archean gold mineralization in the Yilgarn Craton of Western Australia: an overview of the late-orogenic structurally controlled gold deposits. Ore Geol. Rev. 13, 29–64.